

Electronic Supplementary Material (ESI) for Journal of Materials Chemistry A.

This journal is © The Royal Society of Chemistry 2019

Suppression of Surface Defects to Achieve Hysteresis-Free Inverted Perovskite Solar Cells via Quantum Dots Passivation

Chintam Hanmandlu,^{a,b} Satyanarayana Swamy,^{a,c} Anupriya Singh,^{a,c} Hsin-An Chen,^a Chi-Ching Liu,^a Chao-Sung Lai,^{b,d,e*} Anisha Mohapatra,^{a,b} Chun-Wei Pao,^a Peilin Chen,^a Chih-Wei Chu^{a,f*}

^aResearch Center for Applied Science, Academia Sinica 128, Academia Road, Taipei 11529, Taiwan (R.O.C.).

^bDepartment of Electronic Engineering, Chang Gung University, Wenhua First Road, Guishan District, Taoyuan City, 33302, Taiwan (R.O.C.).

^cNano-Science and Technology Program, Taiwan International Graduate Program, Academia Sinica, Taipei 115, Taiwan (R.O.C.).

^dDepartment of Nephrology, Chang Gung Memorial Hospital, Linkou, New Taipei City 33305, Taiwan (R.O.C.).

^eDepartment of Materials Engineering, Ming Chi University of Technology, 84 Gungjuan Road, Taishan, New Taipei City, 24301, Taiwan (R.O.C.).

^fCollege of Engineering, Chang Gung University, No. 259, Wenhua First Road, Guishan District, Taoyuan City 33302, Taiwan (R.O.C.).

Experimental Section

Materials: All chemicals were purchased in their percentage of purity as listed. Lead iodide (PbI_2 , 99.9985%) and lead chloride (PbCl_2 , 99.999%) were purchased from Alfa Aesar. MAI was synthesized according to previous reports [1]. *N,N*-Dimethylformamide (99.8%) and 2-propanol (99.5%) were purchased from Sigma–Aldrich. PEDOT:PSS, PCBM, and C_{60} were purchased from Sigma–Aldrich and used without further purification. The following chemical were purchased from their listed suppliers: cadmium oxide-99% (CdO , Sigma–Aldrich), zinc acetate-99% [$\text{Zn}(\text{OAc})_2$, Sigma–Aldrich], selenium powder (Sigma–Aldrich), hexamethyldisilathiane [$(\text{CH}_3)_3\text{Si})_2\text{S}$, Sigma–Aldrich], dimethyl zinc (DMZ, Merck), oleic acid (OA, Sigma–Aldrich), 1-octadecene-90% (ODE, Acros Organics), sulfur powder-99% (S, Sigma–Aldrich), trioctylphosphine (Sigma–Aldrich), chloroform (J. T. Baker), acetone (J. T. Baker), and MeOH (J. T. Baker).

CdS/ZnS QDs Preparation

The CdS/ZnS QDs with emission frequency at 450 nm in the visible range were prepared with modifications of the procedures described by Zhong et al. and Zhai et al., by varying the percentage of the precursor in the reaction mixture [2]. Two reaction mixtures were prepared, each in a three-necked flask. In one flask (Sol A), 9 mM $\text{Zn}(\text{OAc})_2$ and 0.9 mM CdO were added along with OA (7 mL); the reactants were heated at 80 °C for 1 h under vacuum; 1-ODE (15 mL) was added and the mixture was subjected to N_2 purging. In the second flask (Sol B), 2 mM S powder was dissolved in 1-ODE (8 mL) and then the mixture was heated at 60 °C for 30 min under N_2 purging. Sol A was heated at 280 °C with N_2 purging; Sol B (4.0 mL) was added into Sol A via syringe pump. Syringe pump allow the reaction for 3-4 hours to overgrow the ZnS shell. The reaction was stopped

by removing the heating mantle, followed by addition of excess MeOH at room temperature to precipitate the QDs. The QDs were washed with hexane/MeOH (1:4) 2–3 times to remove the excess surfactants. The powder QDs were stored at 4 °C until required for further use.

CdSe/ZnS QDs Preparation

TOP-capped CdSe/ZnS QDs were prepared with reference to Dabbousi et al.; these QDs had their emission maximum at 525 nm [3]. 1 mM CdOAc and 10 mM ZnOAc were added in three-neck flask with ODE (10 mL) and OA (2.5 mL) to give reaction mixture 1 (RM1). Selenium (ca. 1 M) in TOP (10 mL) was added in another three-neck flask to give reaction mixture 2 (RM2). RM1 and RM2 were subjected to a vacuum to remove atmospheric gases, followed by N₂ purging for 1 h. RM1 was heated at 280 °C and RM2 at 100 C; RM2 (ca. 1.5–2 mL) was added into RM1 via syringe pump. After heating the mixture for 15 min at 280 °C, the heating mantle was removed and the mixture was cooled to room temperature. The QDs were washed with acetone. To prepare the ZnS shell, the method described by Hsia et al., using (CH₃)₃Si)₂S and DMZ, was employed [4]. The QDs were stored at 4 °C until required for further use.

Ligand exchange of QDs (CdSe/ZnS, CdS/ZnS)

Here, we have adopted the previously reported phase transfer exchange to remove the long chain alky ligand capped on QDs [5-7]. For iodide exchange 2 mL of QDs (CdSe/ZnS, CdS/ZnS) dispersed in hexane (15 mgml⁻¹) were added to dimethyleformamide which contain 130 mg of PbI₂ and 47 mg of MAI. After vigorous stirring for 10 min, the QDs are transfer to top hexane phase to bottom DMF phase. After removing the hexane, we washed the QDs solution 2-3 times with hexane to remove the organic residue. Afterwards, the QDs were precipitated using centrifuged solution at 6000 rpm for 2 min. The QDs products were dispersed CF for further use. The J-V

parameters of PSCs devices passivated with CdSe/ZnS and CdS/ZnS without changing of organic ligands exchange as shown the in the Figure S23 and Table S6. The less performance of the device occurred due to an organic ligand on the surface of quantum dots (QDs) impede the carrier motions.

***J-V* and EQE measurements:** All devices were tested under 1-sun conditions and illuminated inside the glove box by using a Xe lamp as a solar simulator (Thermal Oriel 1000 W), which provided a simulated AM 1.5 spectrum (1 sun = 100 mW cm⁻¹). The light intensity was calibrated using a monosilicon photodiode with a KG-5 color filter (Hamamatsu). For the *J-V* curves, the reverse scan was performed from V_{oc} to J_{sc} (from +1.2 to -1 V) and the forward scan from J_{sc} to V_{oc} (from -1 to +1.2 V). The devices were encapsulated before they were removed from the glove box to measure EQE spectra. The light source was a 75-W Xe lamp (Enlitech, QE-R3011); the light output from the monochromator was focused on the photovoltaic cell being tested in DC mode operation.

XRD: X-ray diffraction patterns were recorded at room temperature using a PANalytical-X'Pert X-ray diffractometer (2θ range: 10–60°; step size: 0.008°) equipped with a diffracted beam monochromator set for Cu K α radiation ($\lambda = 1.54056 \text{ \AA}$). The perovskite films and the perovskite films presenting the passivation layers were prepared on ITO/PEDOT:PSS surfaces for measurement.

AFM: Tapping-mode atomic force microscopy was performed for the ITO/PEDOT:PSS/perovskite and ITO/PEDOT:PSS/perovskite/passivation layers (various amounts of CdSe/ZnS QDs in chloroform) using a Bruker AFM system. The Pt/Ir coated tips had a spring constant of 0.5 N/m and were operated at resonant frequencies of 120 kHz. The

preparation of the samples of perovskite films and the perovskite films with passivation layers was as described above.

SEM: Scanning electron microscopy images were recorded using an FEI Noval 200 scanning electron microscope (15 kV). The perovskite films presenting passivation layers were prepared on the ITO/PEDOT:PSS surface for measurement, which The measurements were carried out was performed at room temperature.

Transmittance and absorption: The transmittance and absorption of the perovskite films and the perovskite films presenting various CdSe/ZnS layers were measured using a Jacob V-670 UV–Vis spectrometer. The perovskite films and perovskite films with passivation layers were prepared on glass substrates. These measurements were performed at room temperature.

Impedance spectroscopy: Impedance spectra of the MAPbI₃ devices were measured using a solartron impedance analyzer. The fabrication of the devices was performed as described above. All devices were encapsulated prior to measuring their impedance spectra. The data were analyzed using the program Zview.

XPS: XPS was performed using a PHI 5000 Versa Probe apparatus equipped with an Al K α X-ray source (1486.6 eV). The perovskite films and perovskite films presenting CdS/ZnS and CdSe/ZnS passivation layers were prepared on glass substrates. Perovskite and perovskite/CdSe/ZS samples with Ag electrodes were also prepared on glass substrates and exposed to air for 5 hours at a relative humidity of 85%.

TEM: Transmission electron microscopy was performed using a JEM-2100F microscope (JEOL) installed at the Institute of Physics in Academia Sinica. The particle sizes of the CdS/ZnS and

CdSe/ZnS QDs were measured using TEM. EDS analysis was performed at the Cd L-edge, Se L-edge, Zn K-edge, and S K-edge.

TPC measurement: The transient photocurrent signal was amplified using a TMT variable gain high-speed current amplifier and recorded using a Tektronix oscilloscope (DPO3050). The devices were encapsulated and measured in the dark and at room temperature.

SCLC: Space charge-limited current measurements were performed using electron-dominated devices having the device structure FTO/TiO₂/perovskite (prepared using the inter-diffusion method; with or without CdSe/ZnS QDs)/C₆₀ (20 nm)/BCP (8 nm)/Ag (120 nm). The fabrication procedures for the perovskite and the PCBM and CdSe/ZnS passivation layers in the electron-dominated device are same as those described above; Ag (120 nm) was deposited through thermal evaporation at a deposition rate of 1 Å/s. All of the SCLC measurements were performed at a room temperature in glove box in the dark.

TRPL: Fluorescence lifetime decays were obtained under excitation at 485 nm and 2.5 MHz; the signal was focused on a PDM single-photon avalanche diode (SPAD) from MPD and then processed through PicoHarp 300 Time-Correlated Single Photon Counting (TCSPC) data acquisition. The perovskite films and perovskite films presenting CdSe/ZnS QDs of various sizes were prepared at various thicknesses on glass substrates. In the cases of ETL quenching layers on top of the perovskite/PCBM and perovskite/QDs passivation layers, they were deposited at a thickness of 20 nm through thermal vapor deposition. The deposition of the perovskite and passivation layers was performed as described above. All of these TRPL measurements were performed in the dark at room temperature. For calculations of the TRPL decay lifetimes, a bi

exponential model was used in Decay Analysis software to fit the experimental results and extract the lifetimes.

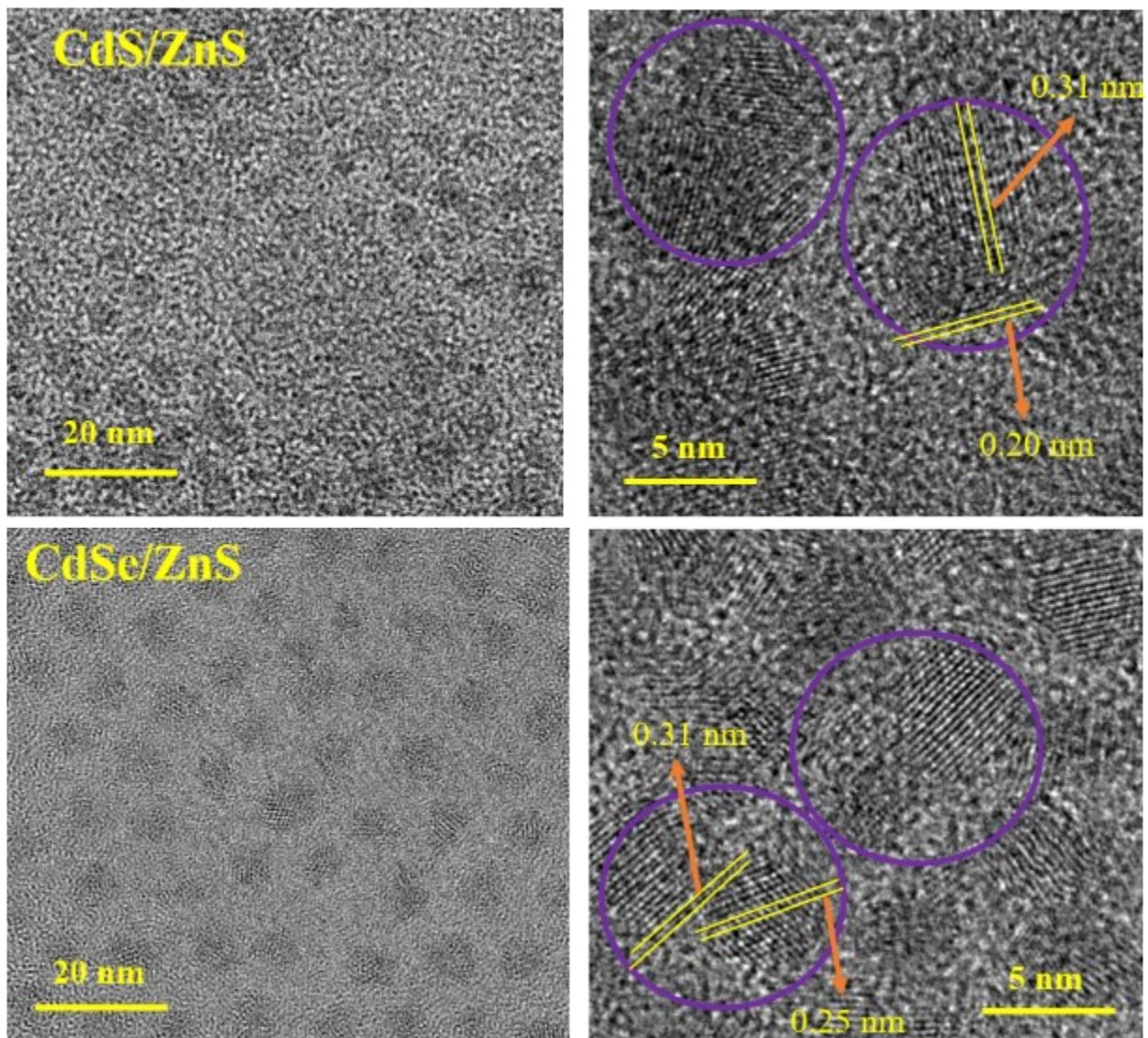


Figure S1: (a, b) TEM images of QDs having dimensions of 4–5 nm: (a) CdS/ZnS; (b) CdSe/ZnS.

The particles in micrographs in **Figure S1**, clearly display crystalline lattice space fringes. The obtained value of d-spacing of CdS/ZnS equal to 0.20 nm corresponding to (111) plane [8], while CdSe/ZnS equal to 0.25 nm corresponding to (111) plane [9]

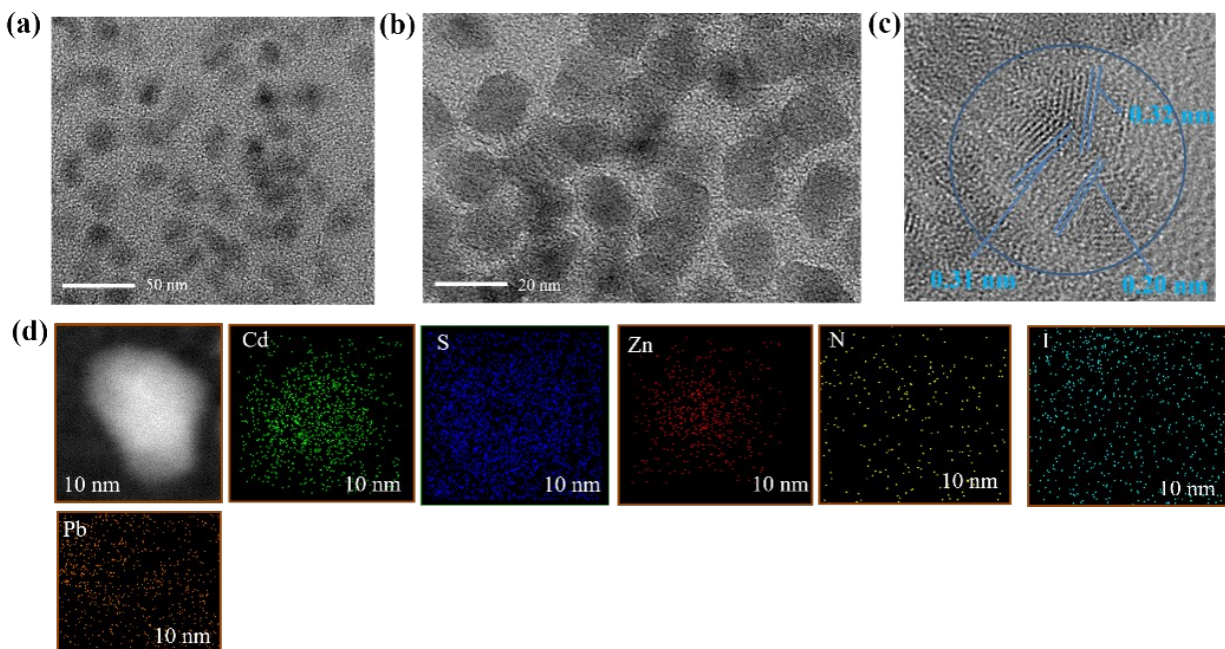


Figure S2: TEM and HRTEM images of CdSe/ZnS QDs after ligand exchange with various magnifications (a) 50 nm (b) 10 nm and (c) 5 nm. (d) Scanning TEM image and EDS mapping, revealing the elemental distributions of the QDs.

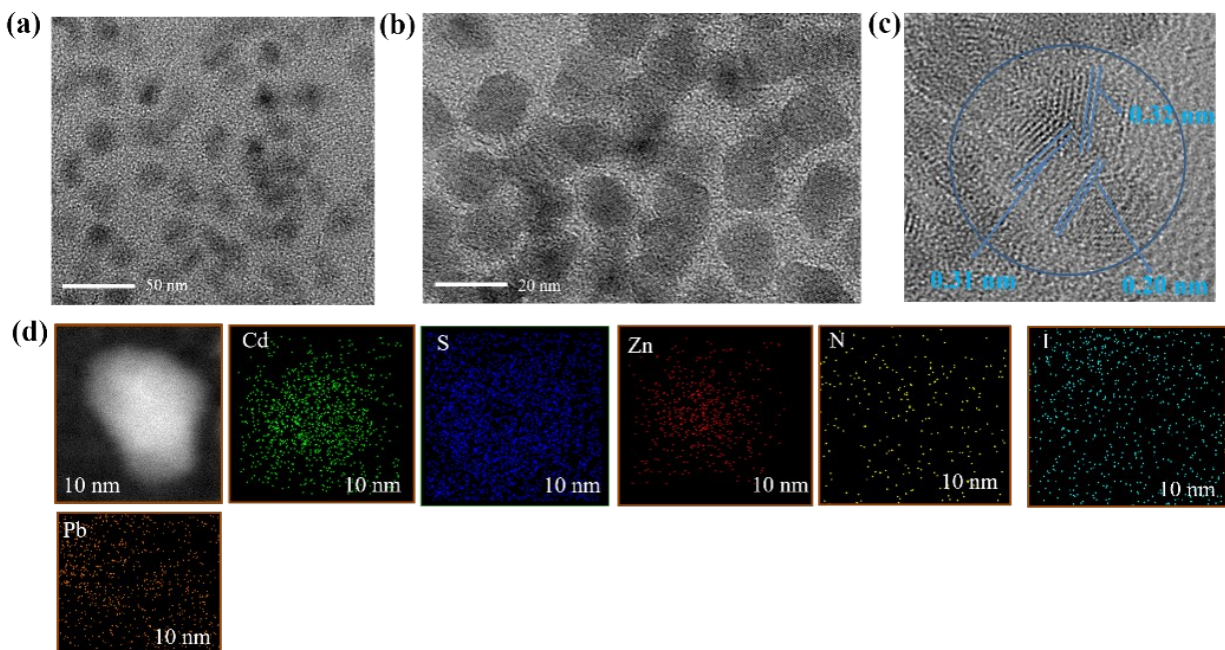


Figure S3: TEM and HRTEM images of CdS/ZnS QDs after ligand exchange with various magnifications (a) 50 nm (b) 10 nm and (c) 5 nm. (d) Scanning TEM image and EDS mapping, revealing the elemental distributions of the QDs.

The organic ligands on QDs provides a good dispersity in non-polar solvents such as hexane as shown in Figure S1. However these long chain organic ligands on would control the carrier motion when the introduced in the solar cells devices, which leads to decrease the performance of the devices. The QDs ligands exchange procedure as discussed in the experimental section. Figure S2 and S3 shows the CdSe/ZnS and CdS/ZnS QDs after iodide ligands exchange. We proposed the CdSe/ZnS and CdS/ZnS QDs in perovskite solids were formed, which is also reported by some other groups [5, 10, 11]. The HRTEM image in Figure S2, S3 shows the lattice fringe spacing of 0.32 nm which corresponds to (004) plane of perovskite [12]. After ligand exchange the CdSe/ZnS and CdS/ZnS QDs maintained the same structure which is confirmed by fringe space (0.20 and 0.25 nm).

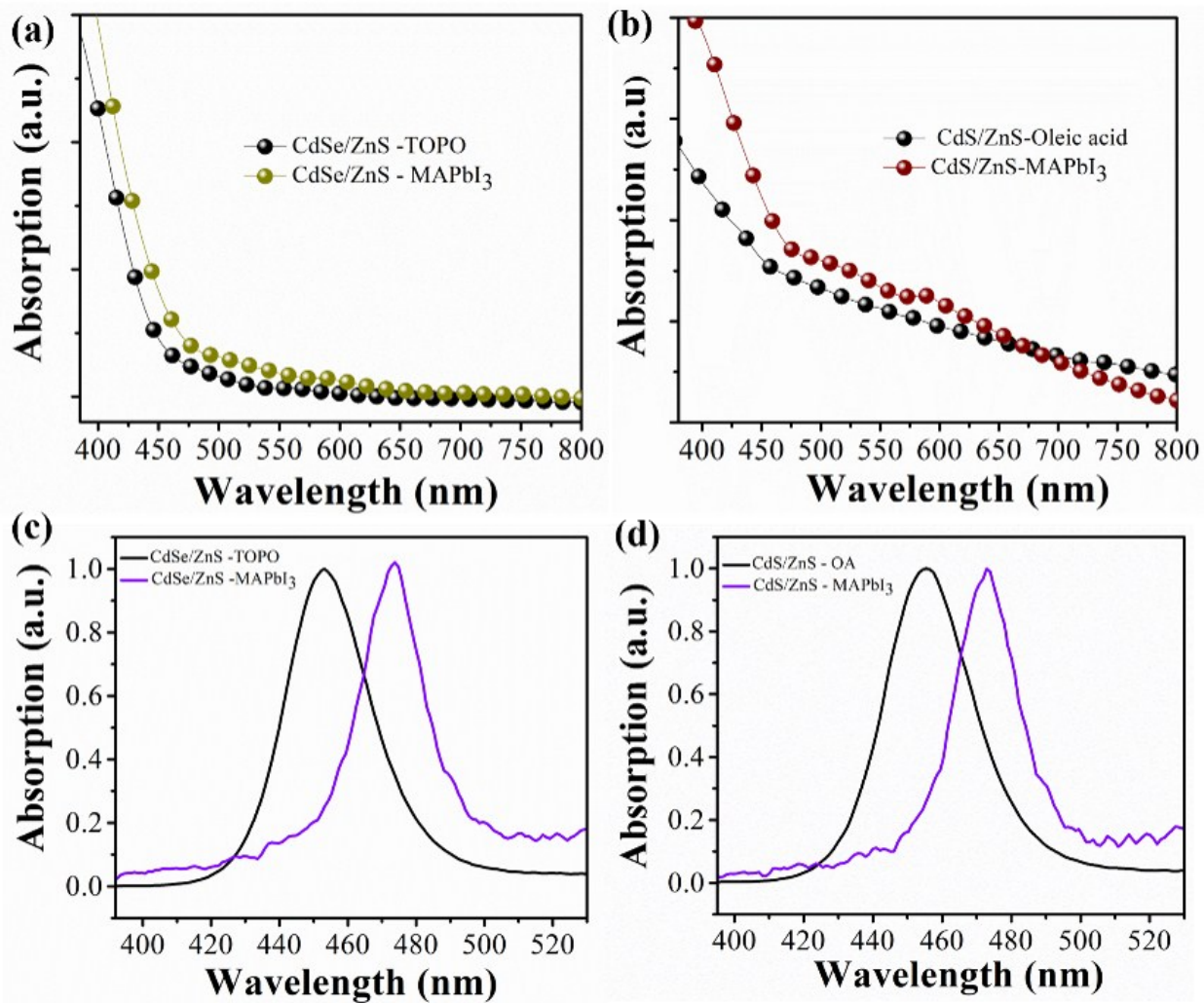


Figure S4: Absorption and PL spectrum of QDs with various ligands (a) CdSe/ZnS (b) CdS/ZnS

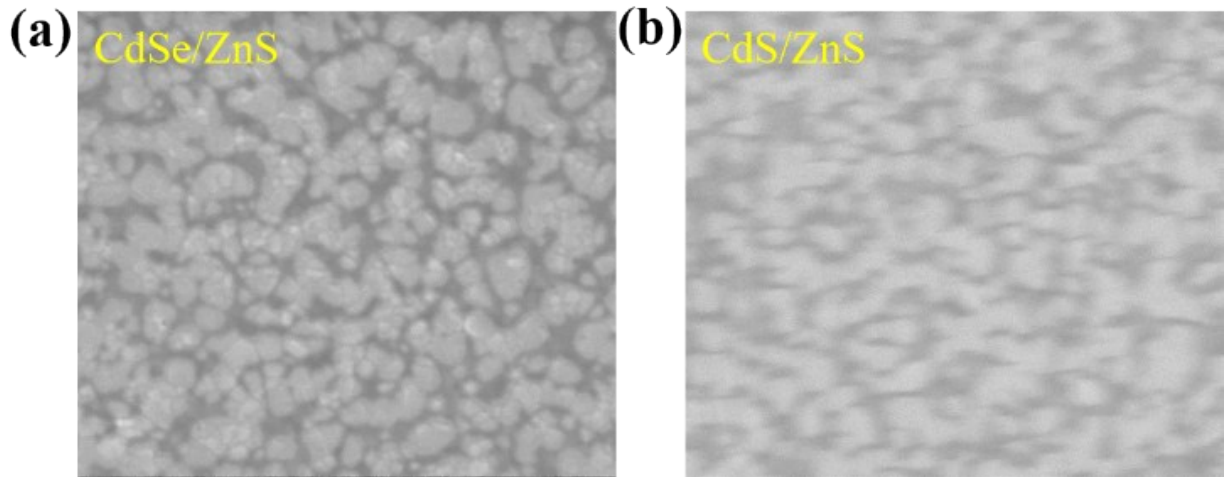


Figure S5: SEM images of perovskite films prepared with 7.5 mg of (a) CdSe/ZnS and (b) CdS/ZnS.

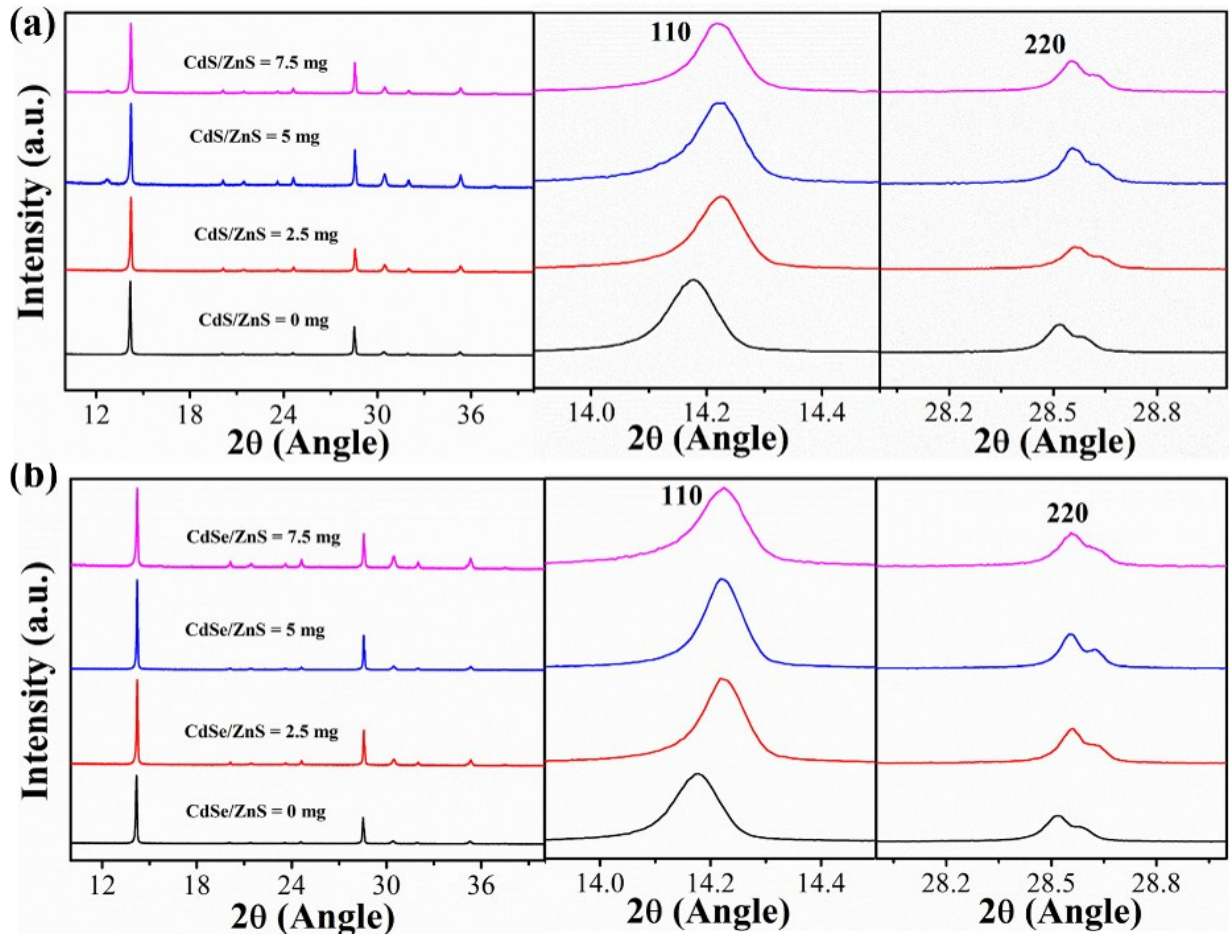


Figure S6: XRD spectra of a perovskite film and perovskite films prepared with various amounts (0–7.5 mg) of QDs: (a) CdS/ZnS; (b) CdSe/ZnS.

In Figure S6, the XRD spectra reveal no systematic variations upon varying the amounts of QDs on the perovskites, with no obvious changes in the perovskite phase. Using the full-wavelength half-maximum (FWHM) to calculate the crystallite sizes of the dominant perovskite phases, the value of the FWHM of the sample without the passivation layer was 0.090, while the sample prepared with various amounts of the CdS/ZnS and CdSe/ZnS passivation layers gave values of 0.082, 0.075, and 0.083 and 0.82, 0.82, and 0.75, respectively, for the (110) and (220) planes, respectively. The calculated FWHMs revealed no significant variations in the samples prepared with or without passivation layers on top of the perovskites.

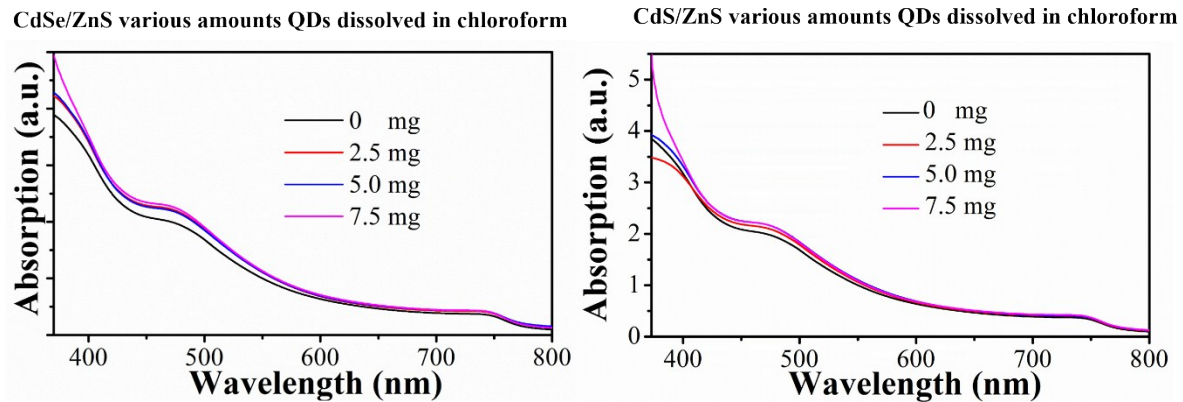


Figure S7: Absorption spectra of perovskite films presenting various QD passivation layers on glass: (a) CdSe/ZnS and (b) CdS/ZnS.

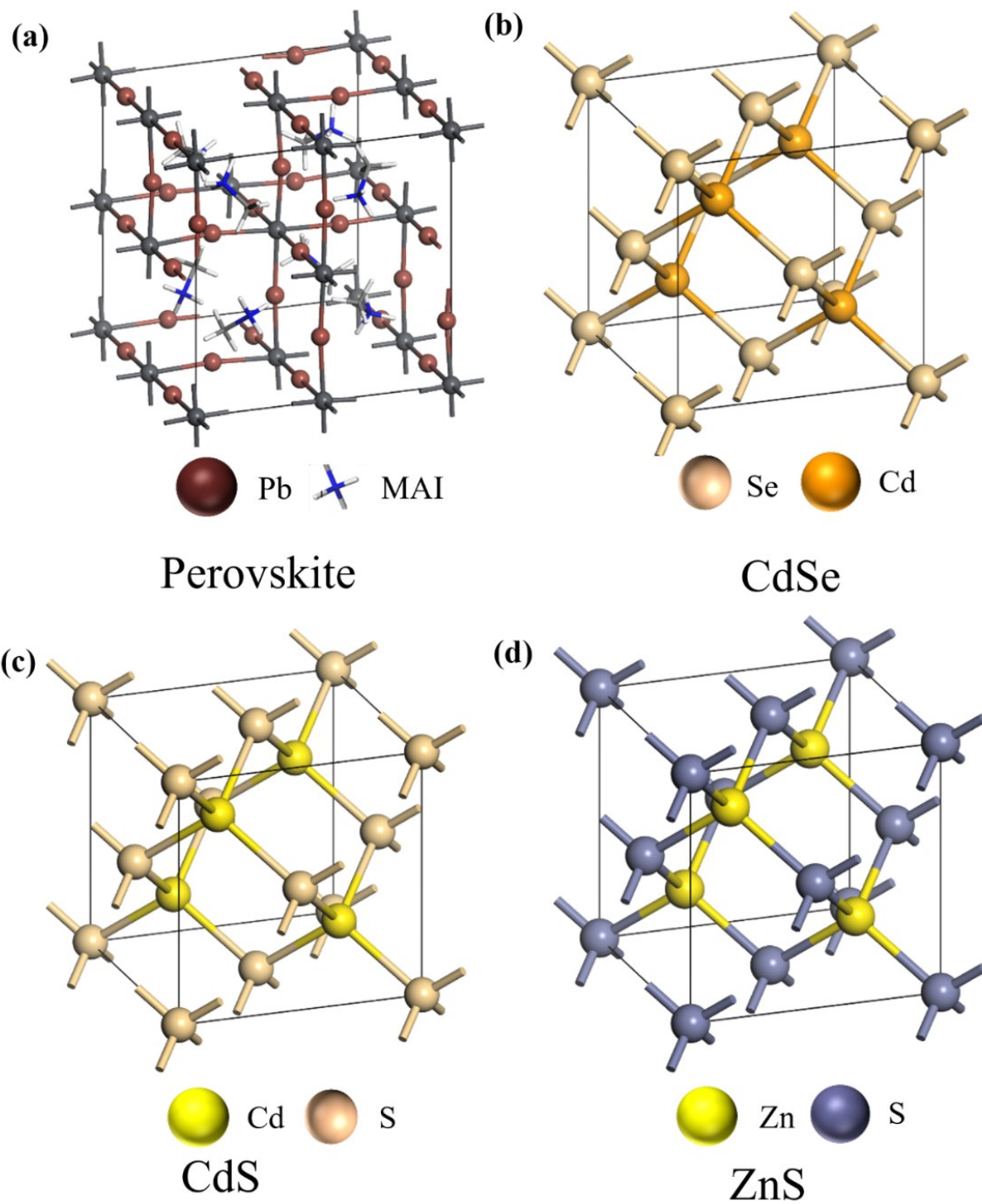


Figure S8: Crystal structures of the photoactive layer and the passivation layers of CdSe, CdS, and ZnS.

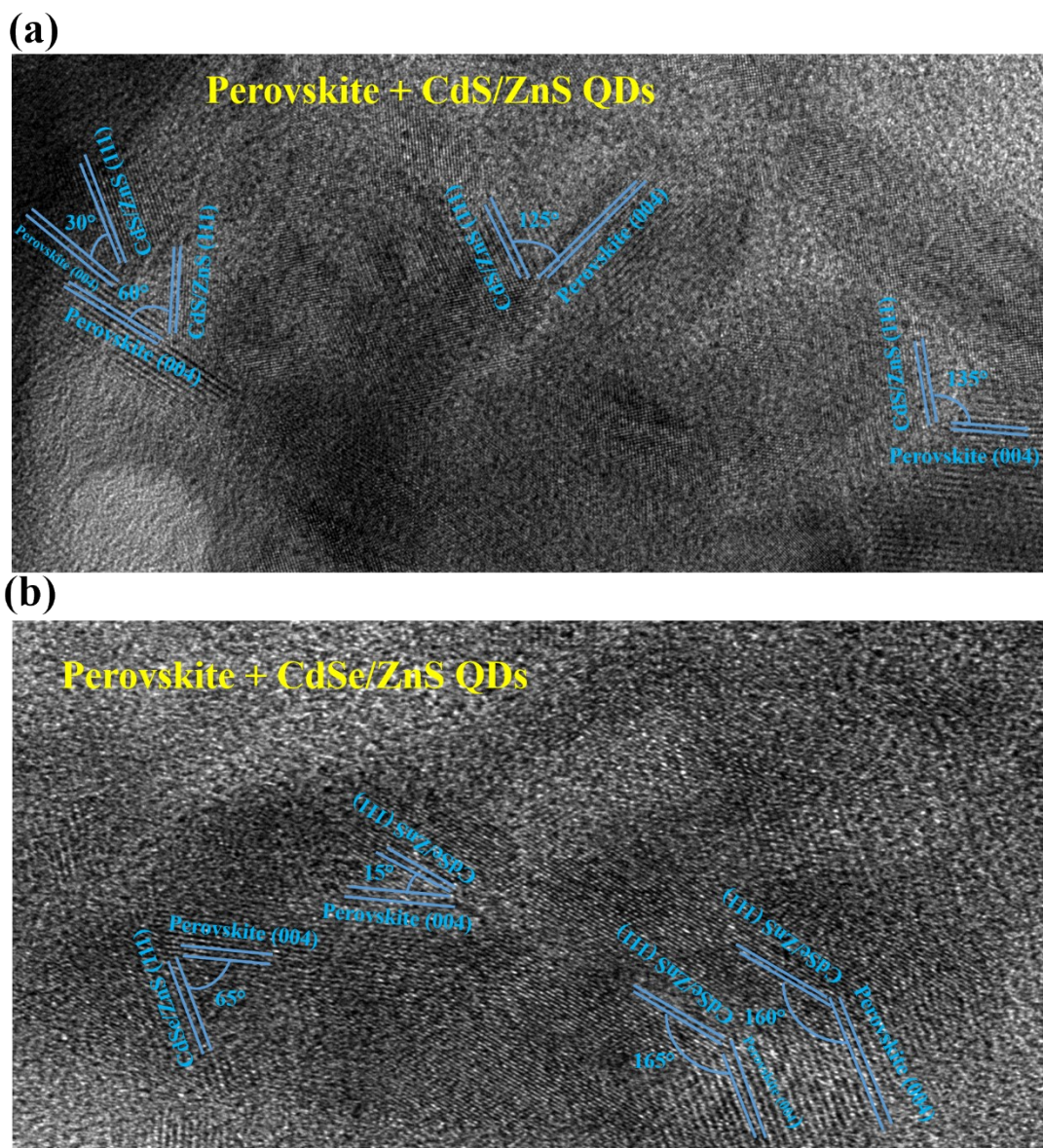


Figure S9: HRTEM image of QDs on perovskite (a) CdS/ZnS (b) CdSe/ZnS.

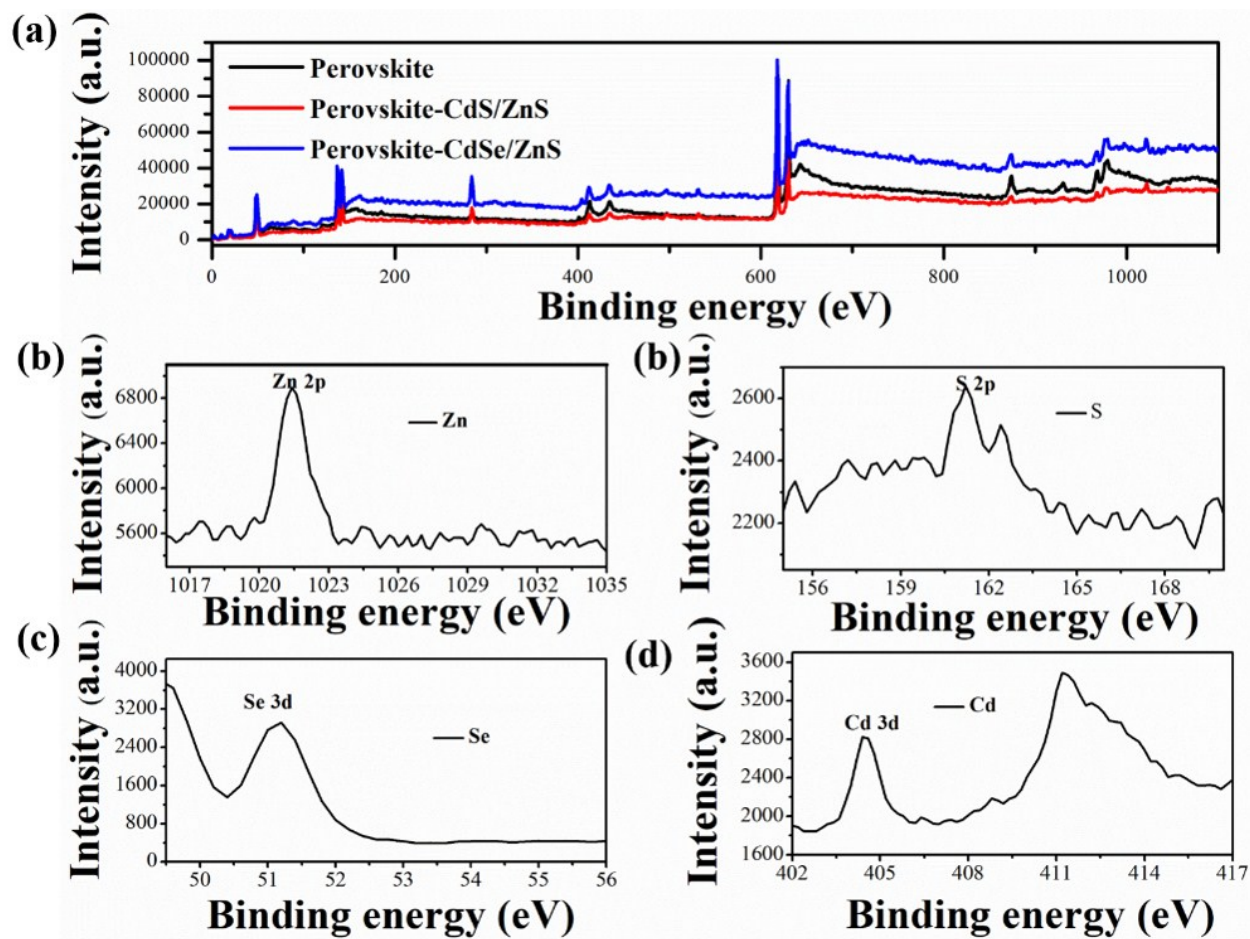


Figure S10: (a) XPS full spectrum of a perovskite film and perovskite films presenting CdS/ZnS and CdSe/ZnS deposited on glass. (b–e) XPS spectra of (b) Zn, (c) S, (d) Se, and (e) Cd.

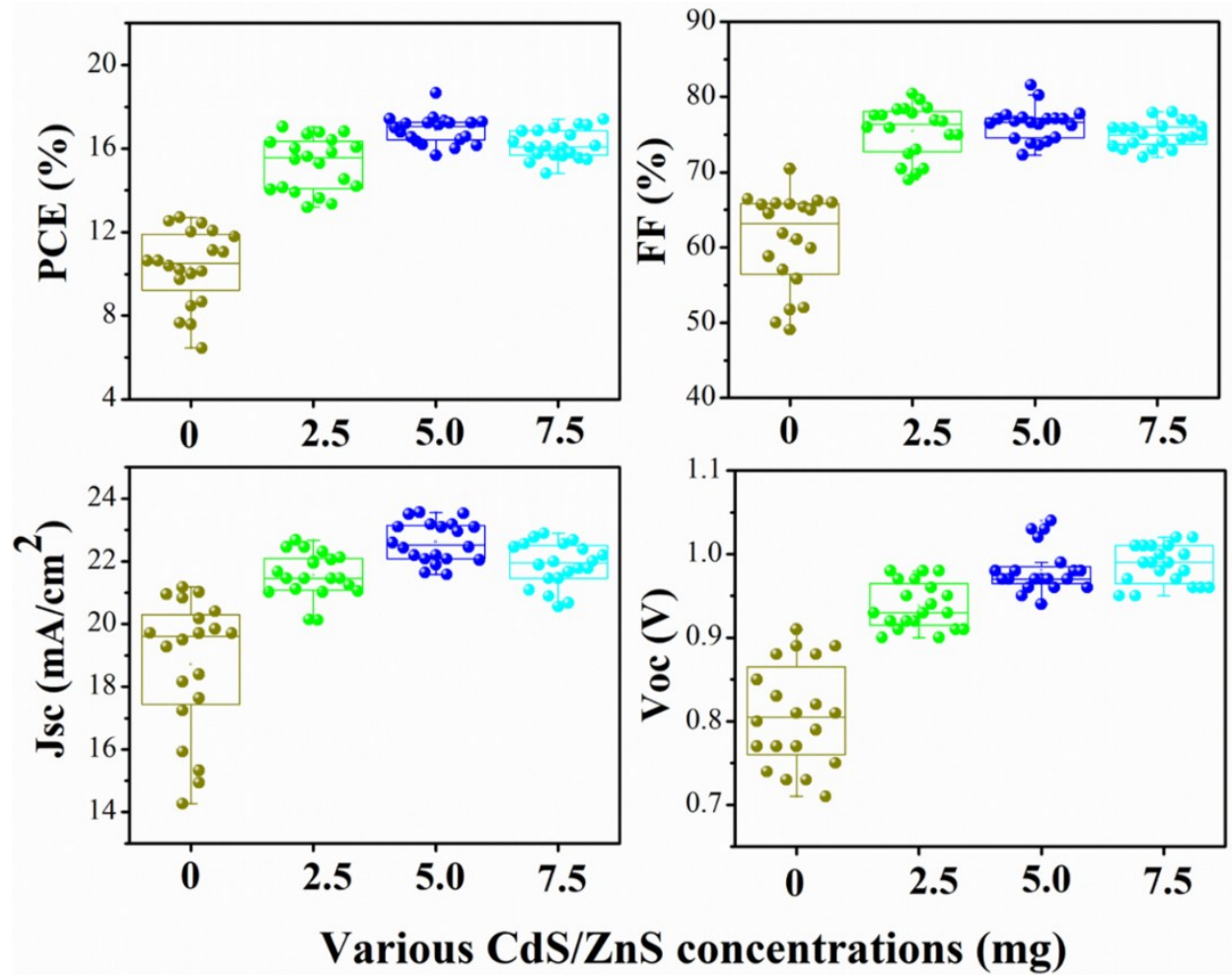


Figure S11: Photovoltaic parameters of CdS/ZnS passivation layers prepared at various concentrations.

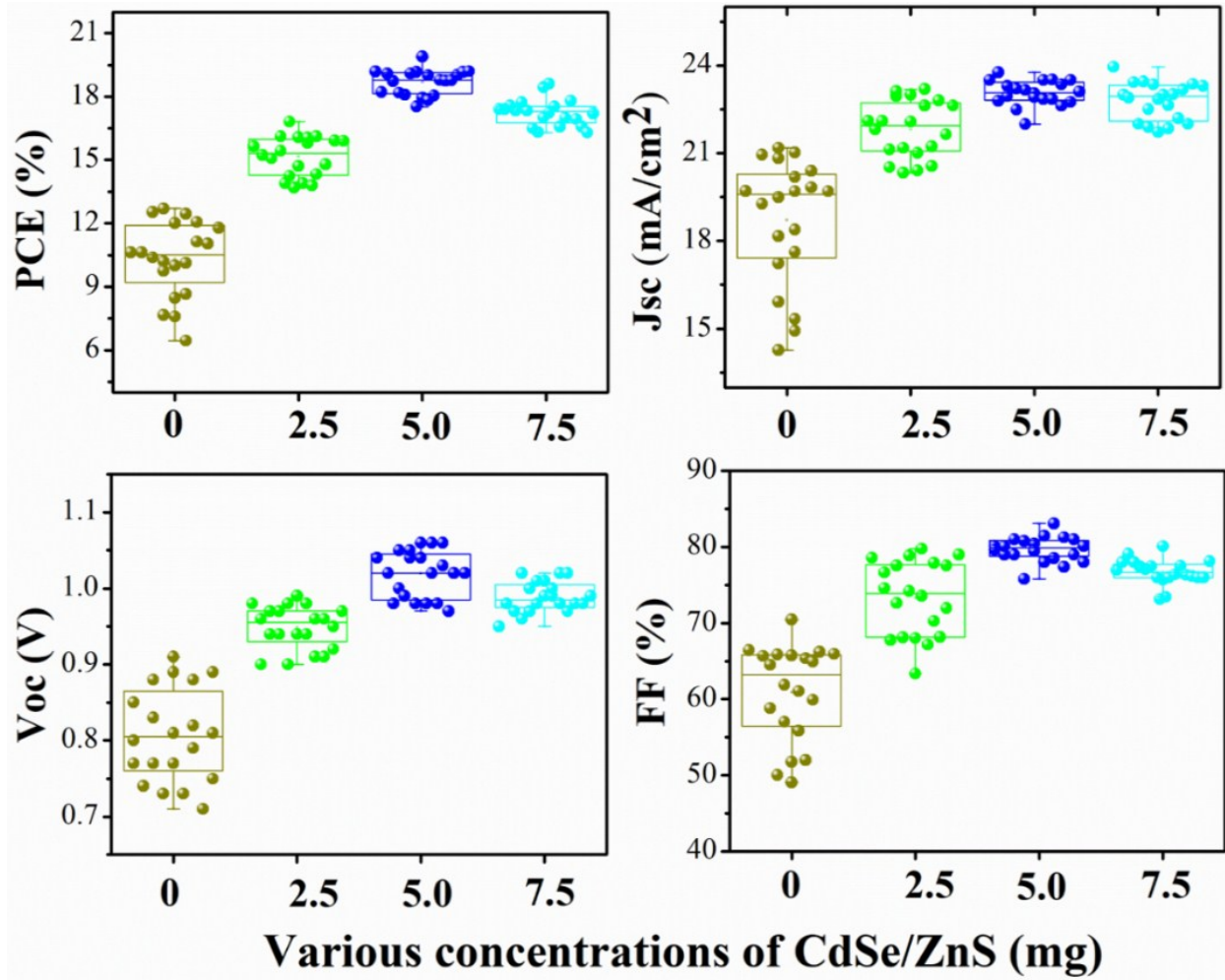


Figure S12: Photovoltaic parameters of CdSe/ZnS passivation layers prepared at various concentrations.

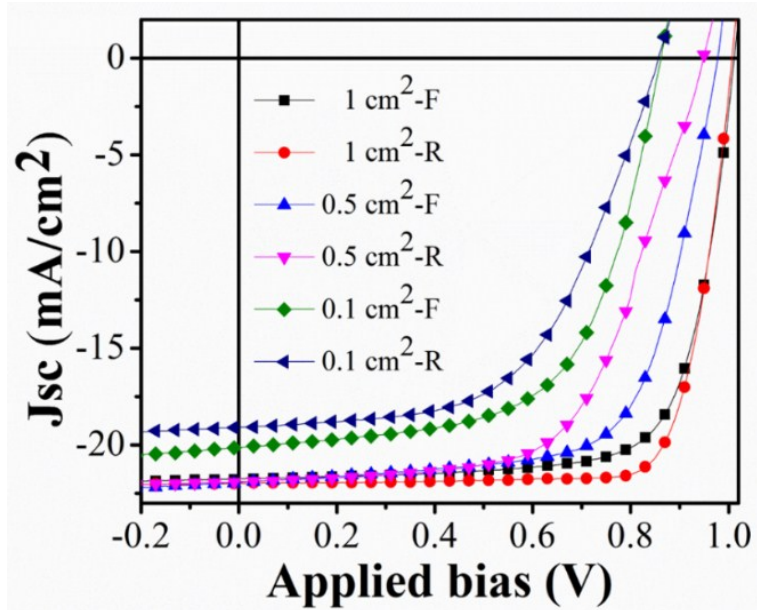


Figure S13: J - V curves of PSCs incorporating a PCBM passivation layer, with active areas of 1, 0.5, and 0.1 cm^2 .

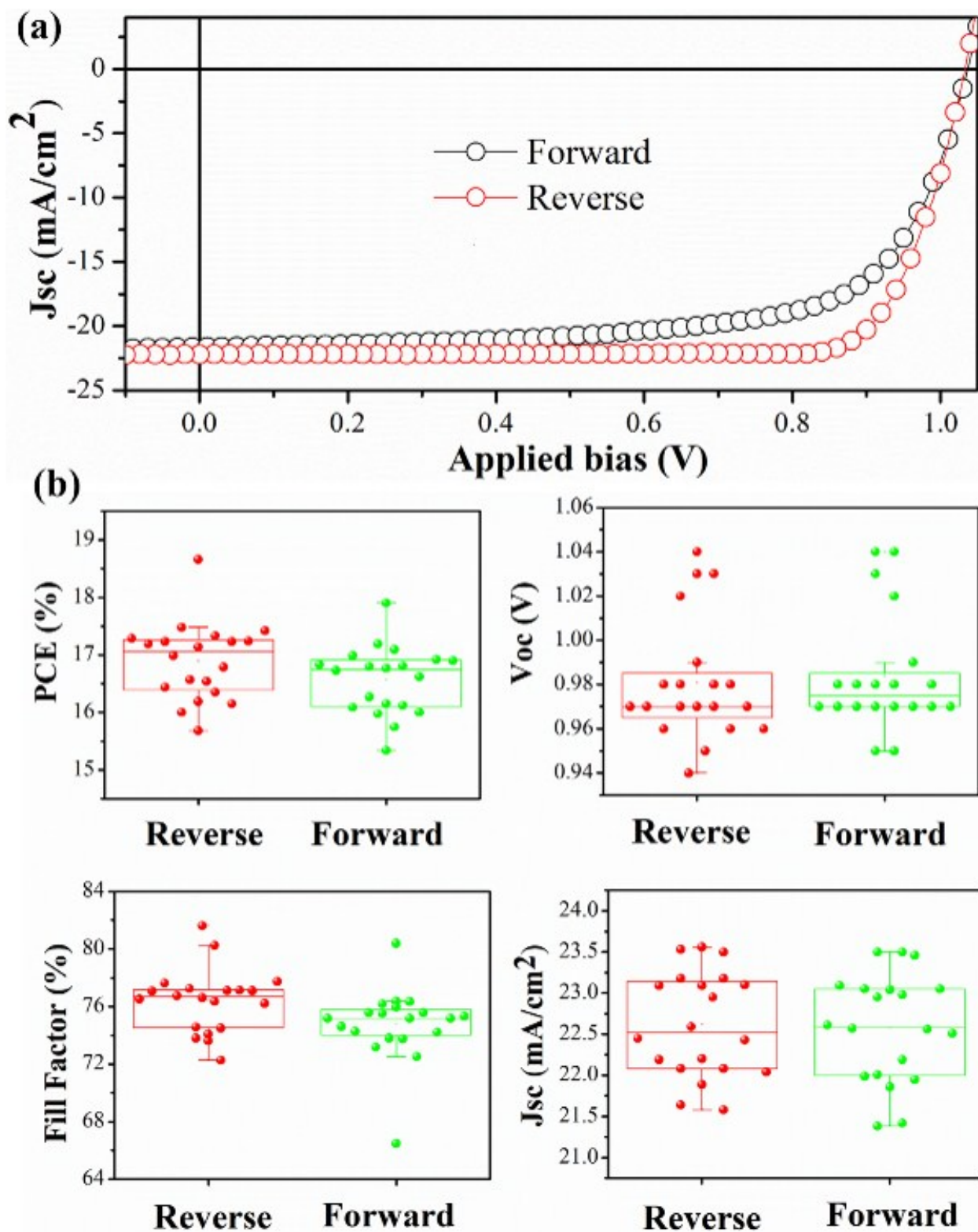


Figure S14: (a) Best device performance based on the CdS/ZnS passivation layer. (b) Statistical

photovoltaic parameters (forward and reverse scan directions) of 20 PSC devices incorporating CdS/ZnS passivation layers.

Figure S14 presents the $J-V$ characteristics of PSC devices incorporating the CdS/ZnS passivation layer. The best cell achieved an efficiency of 18.65%, as presented in Figure S14a, in the reverse scan direction. The statistical distributions of the photovoltaic parameters of the PSC devices are provided in Figure S14b. The hysteresis in the $J-V$ curves based on CdSe/ZnS was low compared with that of the CdS/ZnS passivation layer. Therefore, it is reasonable to believe that CdSe/ZnS is an efficient passivation layer for hysteresis-free PSCs. The origin of hysteresis in PSCs incorporating the CdS/ZnS passivation layer can be explained by considering the following mechanisms. The hysteresis may also arise from trap states at the interface between the perovskite and CdS/ZnS layers. The surface states of the perovskite were not suppressed after CdS/ZnS passivation, as supported by DFT calculations. In addition, after passivating the surface with CdS/ZnS and CdSe/ZnS layers, the perovskite binding energies were 0.093 and 0.083 eV/A², respectively. The lower binding energy can be attributed to the electronegativity of the S²⁻ anions from CdS/ZnS being higher than that of the Se²⁻ ions from CdSe/ZnS when interacting with the Pb atoms of the perovskite. The poorer performance suggests that the S²⁻ anions from CdS/ZnS hindered charge transport in the CdS/ZnS passivated perovskite devices, due to the higher electronegativity. As a result, the presence of the CdS/ZnS passivation layer could create hysteresis in the $J-V$ characteristics of the PSCs.

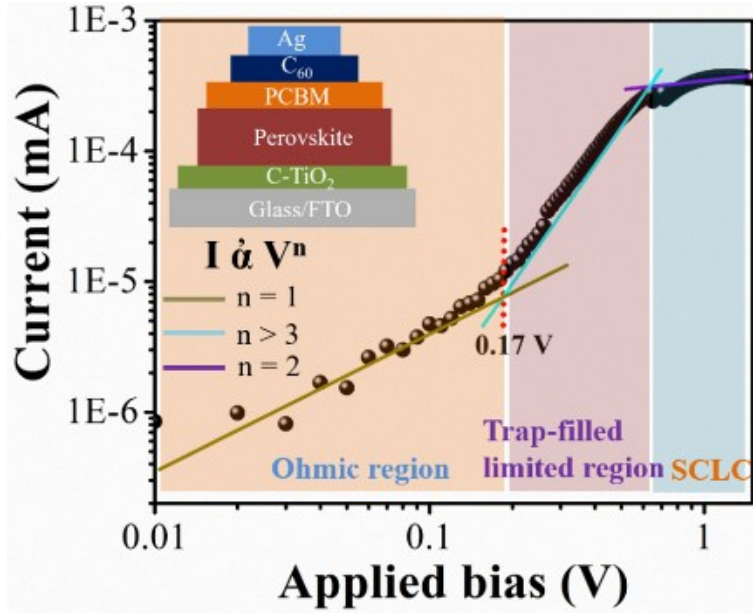


Figure 15: Dark J - V traces of the trap density of perovskite with electron only device.

Supplementary note 1: To calculate the density of defect states in electron-dominated devices without and with PCBM and CdSe/ZnS passivation layers, the space charge-limited current (SCLC) was applied; the device structure was FTO/C-TiO₂/perovskite (with and without CdSe/ZnS QDs, PCBM passivation layers)/C₆₀/Ag. As revealed in **Figure 5a**, there were three regions (ohmic region, trap filled, and SCLC) in the logarithmic plots of the I - V characteristics of the electron-dominated devices incorporating the control and target passivation layers. In the SCLC model, the density of defect states or trap states are estimated roughly from trap filled region the onset of voltage (V_{TFL}). The trap densities of the electron-dominated device were calculated from the following equation:

$$V_{\text{TFL}} = e \times n_t \times d^2 / 2 \times \epsilon \times \epsilon_0$$

where e , n_t , d , ϵ , and ϵ_0 are the electron charge, the trap density, the thickness of the perovskite film, the dielectric constant of the perovskite material, and the permittivity of free space,

respectively [13]. For the control passivation electron-based device, the value was 0.29 V, while for the target passivation layer-based device it was 0.11 V. Using the equation above, we calculated the trap densities; the CdSe/ZnS passivated device had a lower trap density than that of the device prepared with the PCBM passivated. Hence, the results from the SCLC measurements for the PCBM and CdSe/ZnS passivated devices were consistent with those from the steady state PL measurements.

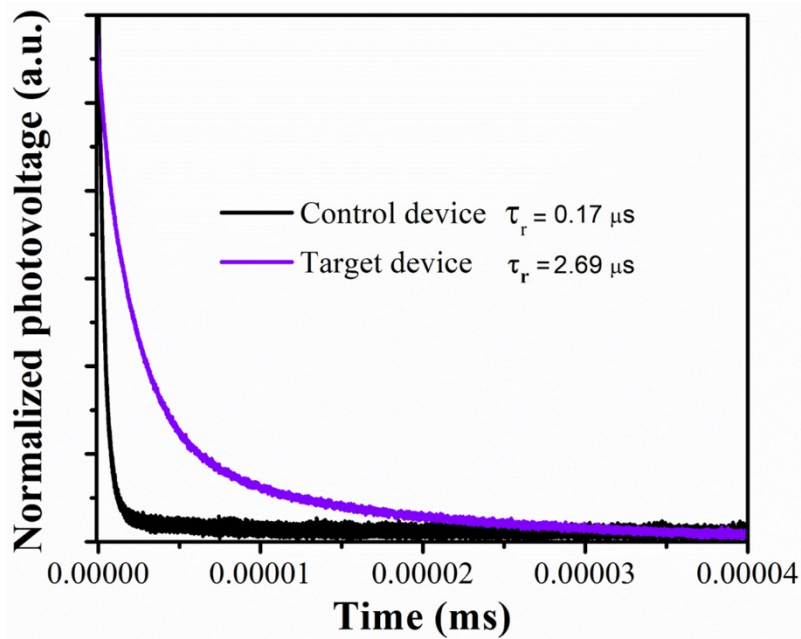
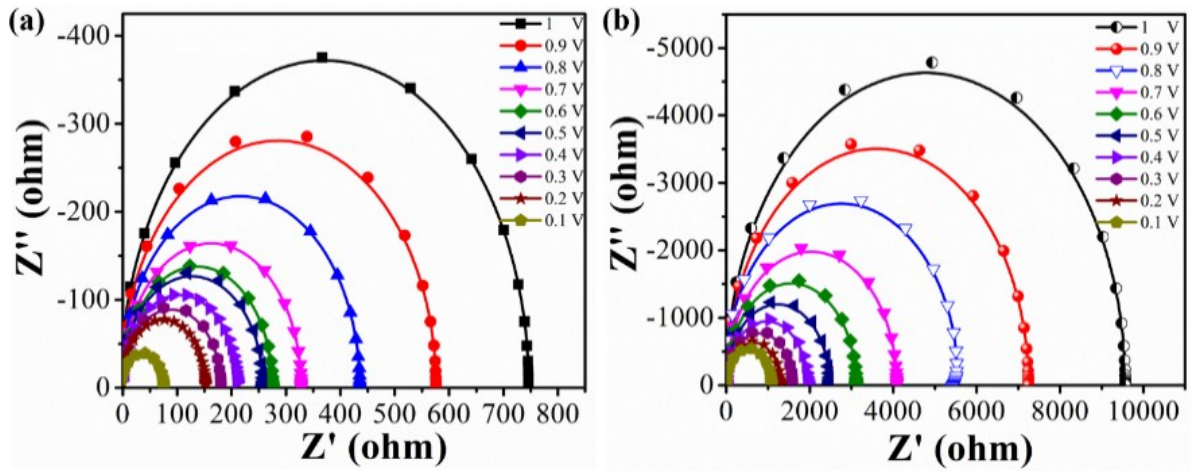


Figure S16: Transient photo decay curves of target and control PSCs devices.



Figure

re S17: Nyquist plots of impedance spectra measured under dark with various bias voltages for the (a) control (b) target PSCs devices.

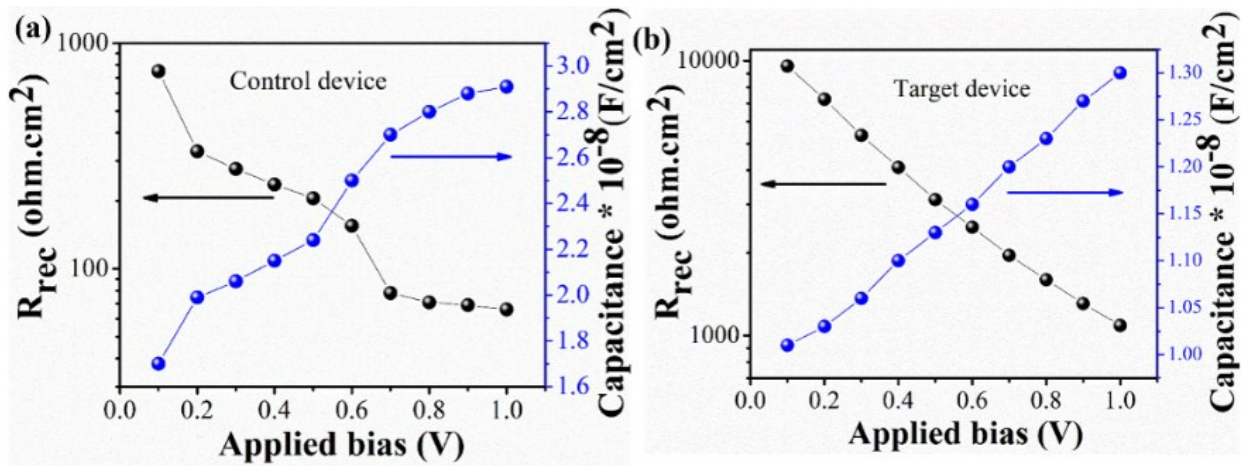


Figure S18: Fitted values of the interfacial recombination resistance (R_{ct}) and chemical capacitance (C_{μ}) of PSC devices (a) control (b) target.

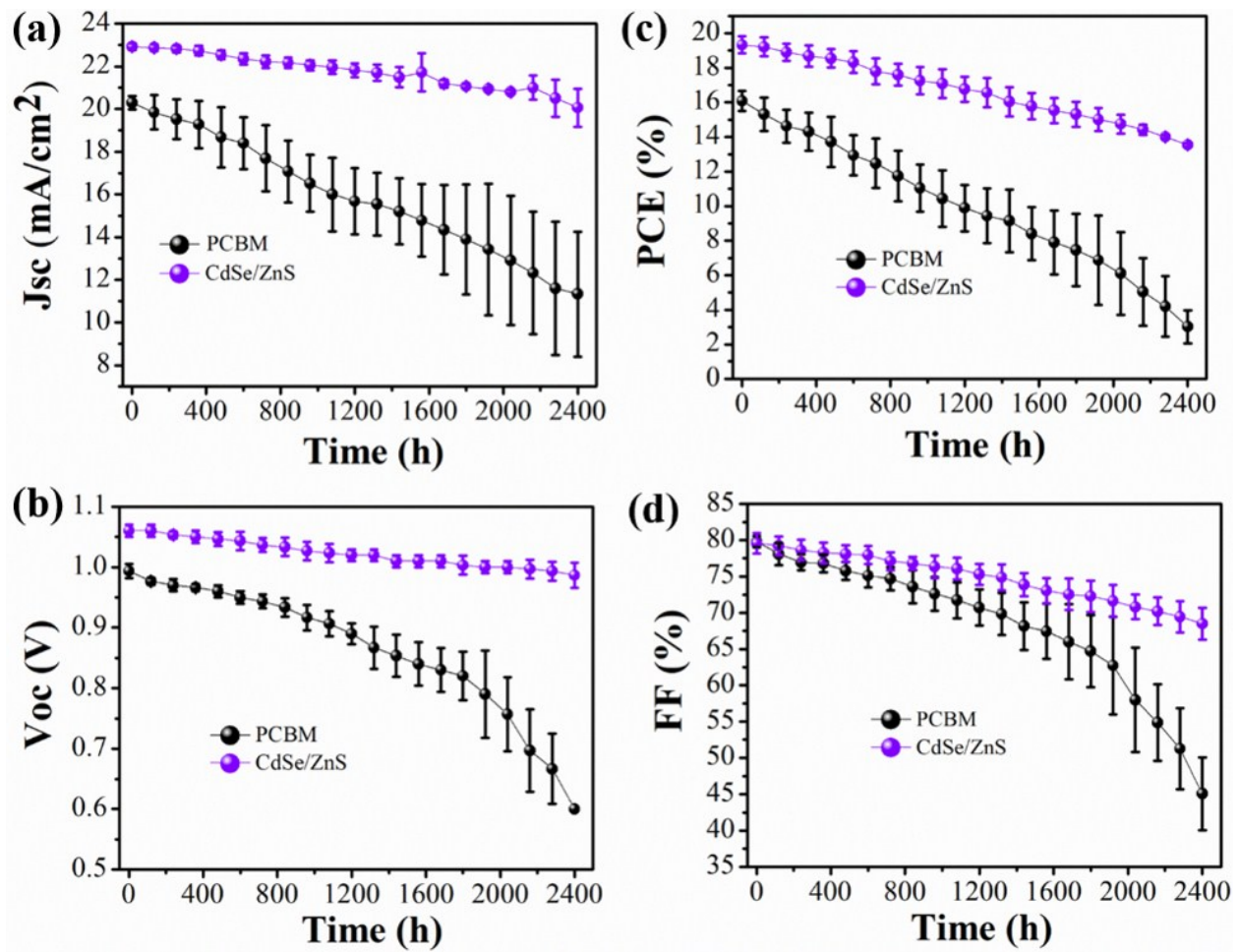


Figure 19: Long-term stability of PSC devices incorporating PCBM and CdSe/ZnS passivation layers. Evolution of the values of (a) J_{sc} , (b) V_{oc} , (c) PCE, and (d) FF, relative to the initial parameters for the devices incorporating PCBM and CdSe/ZnS, measured over 2400 h.

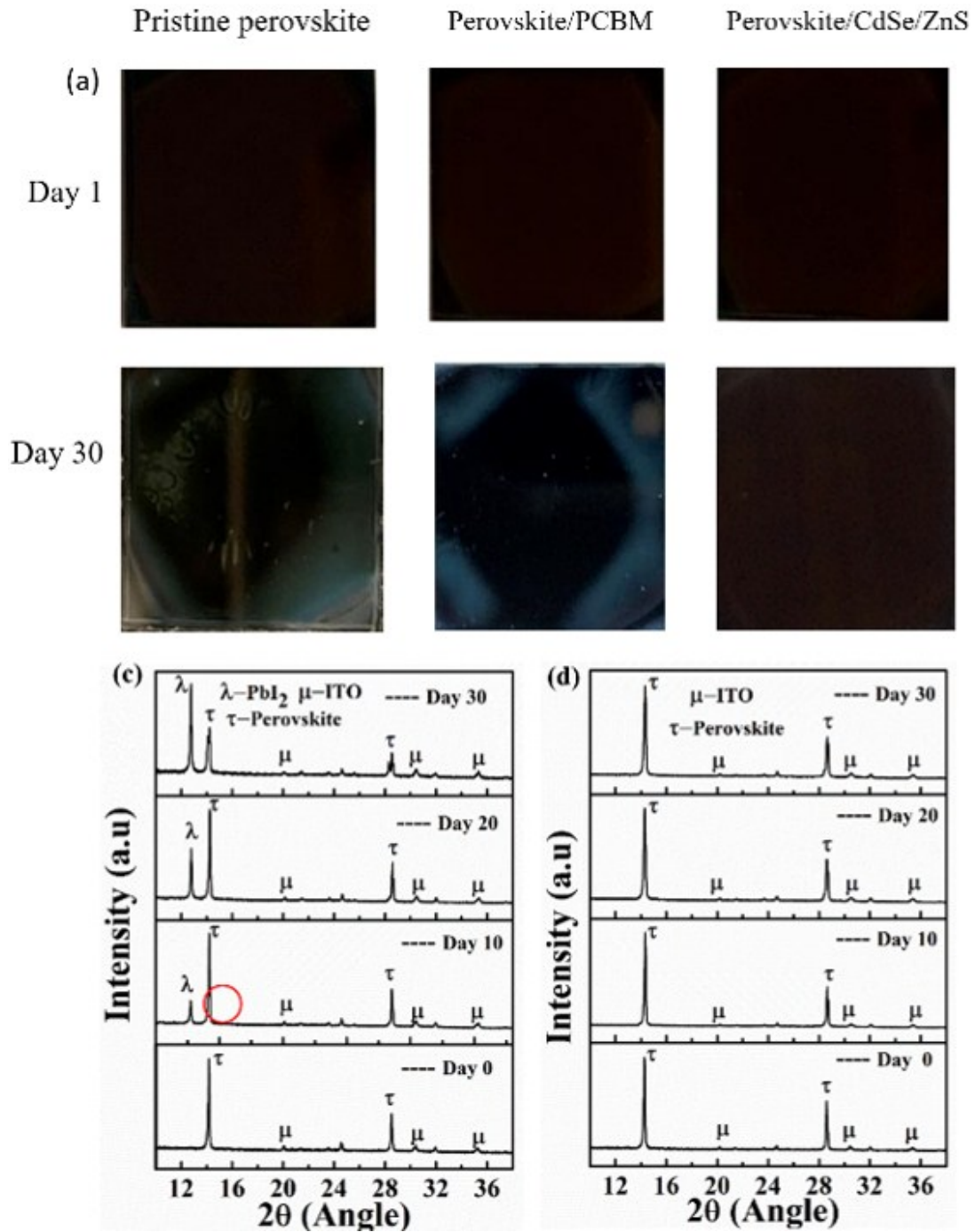


Figure 20: (a, b) Photographic images of pristine and passivated perovskite films before and after 30 days. Identification of the composition of the degraded perovskite film. (c, d) XRD patterns of perovskite films incorporating PCBM and CdSe/ZnS passivation layers.

The humidity stability test for bare perovskite films (Figure S20a,b) shows that the films with CdSe/ZnS passivated have much slower degradation than of pristine perovskite and PCBM passivated they were exposed at room temperature to RH 50-60 %. Figures S20c,d reveal the structural stability of the perovskite materials featuring the PCBM and CdSe/ZnS passivation layers. The perovskite films were exposed at room temperature to RH 50–60% and measured every 10 days. The films based on the PCBM passivation layer began to degrade from 10 days onward; in contrast, the films based on the CdSe/ZnS passivation layer were stable for up to 30 days. The results indicate that the perovskite materials presenting CdSe/ZnS passivated were more stable than those presenting the PCBM passivated.

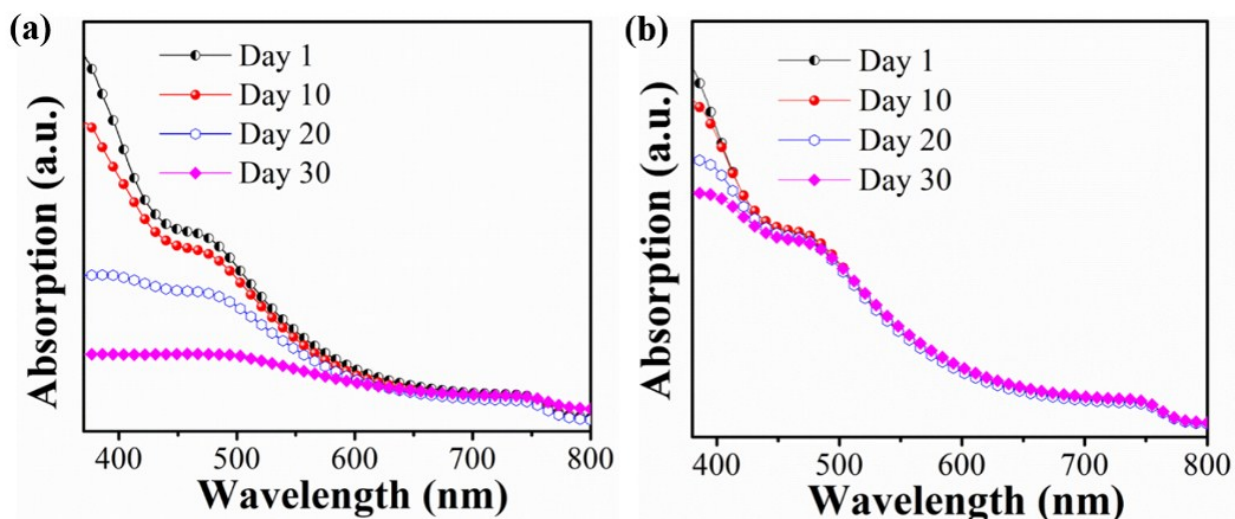


Figure 21: Absorption spectra of perovskite films presenting (a) PCBM and (b) CdSe/ZnS passivation layers.

The Figure S21 reveals the absorption stability of perovskite films presenting the CdSe/ZnS and PCBM passivation layers. The perovskite films were exposed at room temperature to RH 50-60% and measured by every 10 days. The perovskite films passivated with PCBM layers began to degrade from 10 days onward; in contrast, the films presenting the CdSe/ZnS passivated were

stable for over 30 days under the same conditions. The results indicate that the films presenting the CdSe/ZnS passivation layers were more stable than those presenting the PCBM layer.

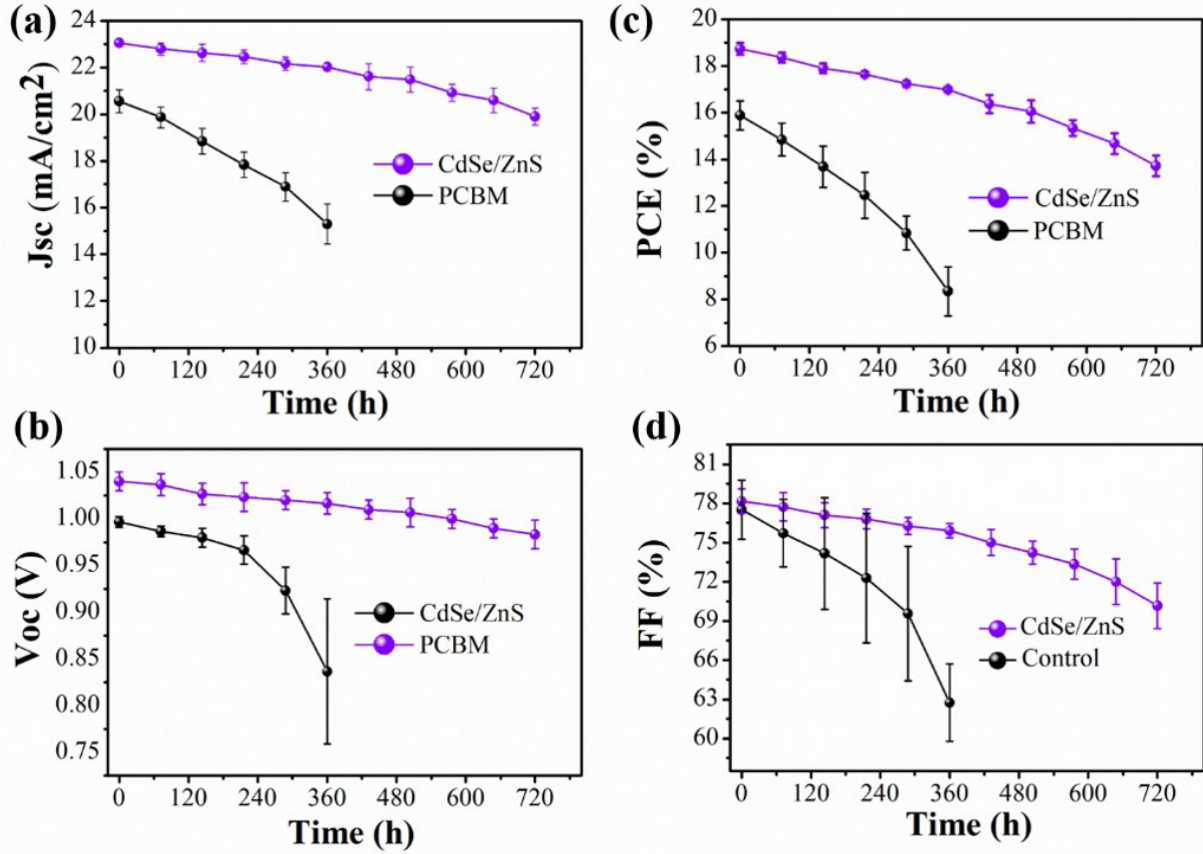


Figure 22: Thermal stability of PSC devices incorporating PCBM and CdSe/ZnS passivation layers. Evolution of the values of (a) J_{sc} , (b) V_{oc} , (c) PCE, and (d) FF, relative to the initial parameters for the devices incorporating PCBM and CdSe/ZnS, measured over 720 h.

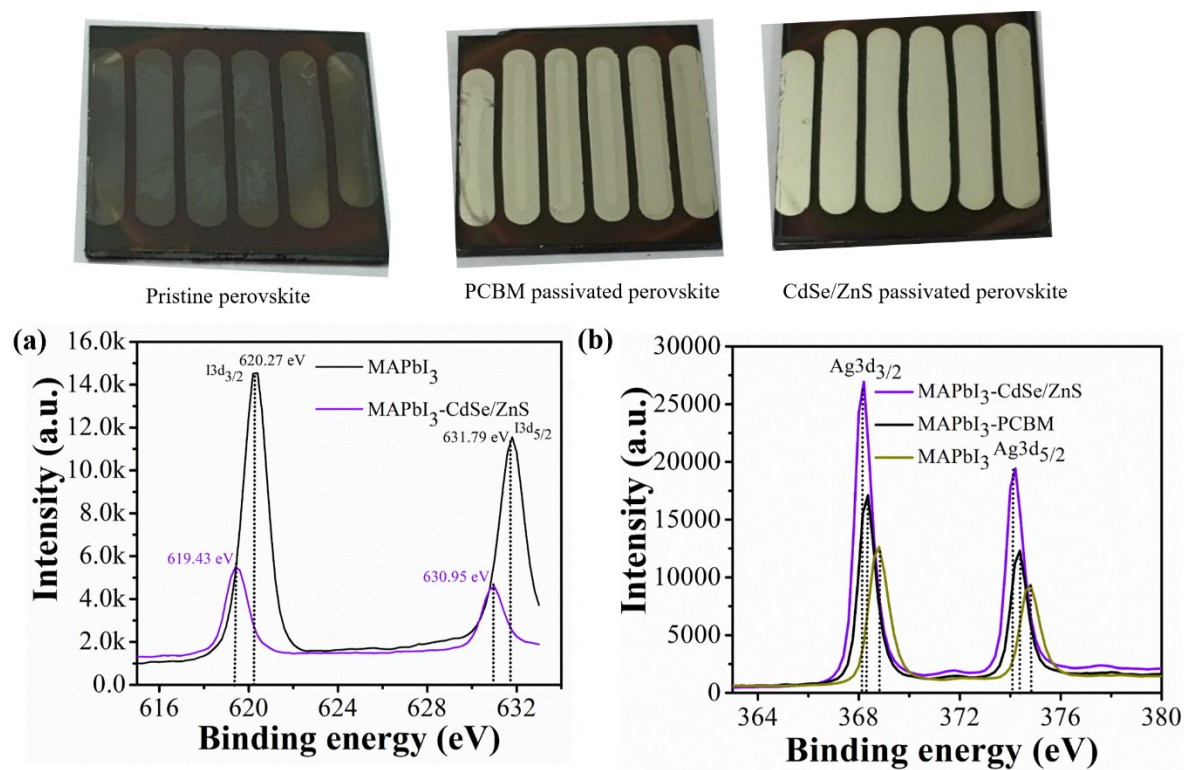


Figure S23: XPS spectra of perovskite films and perovskite/CdSe/ZnS films with a Ag electrode: (a) I 3d and (b) Ag 3d.

Here, we directly deposited the Ag electrode on top of the perovskite film and the perovskite films presenting the target QDs for 2 h at room temperature with 90% RH. We observed, in case of the perovskite presenting QDs, a highly reflective Ag cathode after aging under the atmosphere; in contrast, the perovskite presenting the Ag electrode formed a purple/brown electrode under the same conditions, as displayed in **Figure S23a**. These findings can be explained by considering the diffusion of iodine to the electrode in the perovskite films; after some time, the halogenated silver formed silver iodide, which has large resistivity at the electrode, accounting for the decrease in device performance. The binding energy of iodine increased, implying that iodine was bound directly to the electrode; in contrast, the iodine peak intensity was weaker for the perovskite presenting the PCBM and CdSe/ZnS passivation layers. The CdSe/ZnS QDs suppressed the iodine

diffusion to the electrode because of the strong interaction between the Se^{2-} and MA^+ ions, such that the Se^{2-} anions suppressed the liberal motion of the MA^+ cations. These findings indicate that iodine diffusion to the cathode was suppressed substantially when using the CdSe/ZnS QDs to passivate the perovskite.

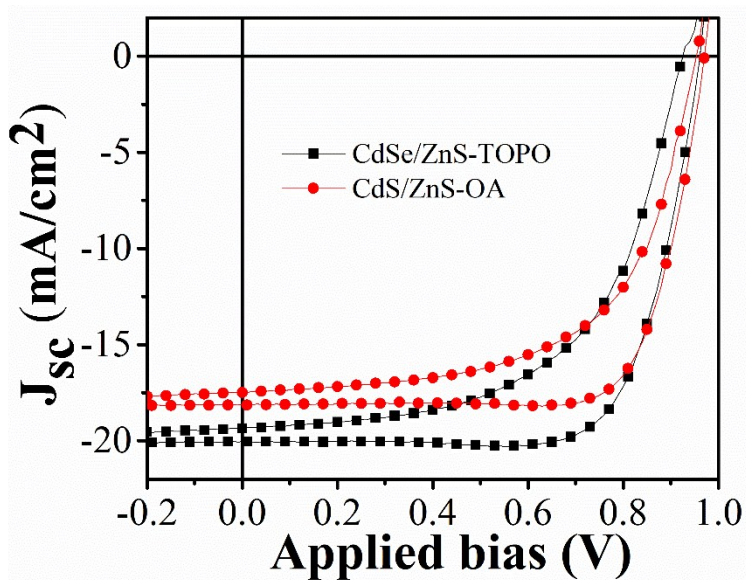


Figure S24: J-V characteristics of PSCs devices with CdSe/ZnS-TOPO and CdS/ZnS-OA passivation layers.

Table S1: Photoelectron binding energies of perovskite, perovskite/CdSe/ZnS, and CdS/ZnS

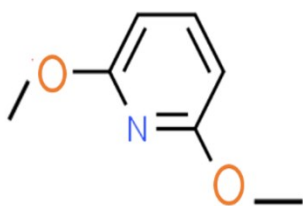
Sample	Pb 4f _{5/2}	Pb 4f _{7/2}	I 3d _{3/2}	I 3d _{5/2}
Perovskite	137.69	142.63	618.54	630.09
Perovskite/CdSe/ZnS	137.25	142.22	618.00	630.09
Perovskite/CdS/ZnS	137.53	142.53	618.52	629.99

Table S2: Time constants in TRPL, determined through exponential fitting, measured for target QDs on perovskite.

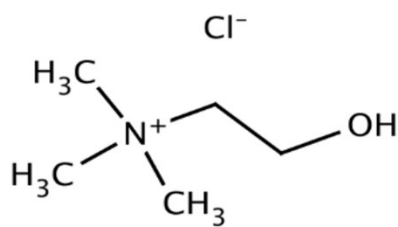
	Perovskite	Perovskite/CdS/ZnS	Perovskite/CdSe/ZnS
A ₁	1248	537	751
Proportion (%)	62.16	58.36	68.41
τ ₁ (ns)	59.05	146.77	170.38
A ₂	759.5	383	346.67
Proportion (%)	37.83	41.63	31.58
τ ₂ (ns)	22.75	53.35	59.73
τ _{average} (ns)	52.15	115.23	155.01

Table S3: Photovoltaic performances of PSC devices reported based on passivation layers.

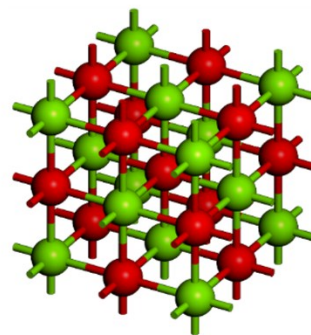
Perovskite/Interface	Scan direction	$\Delta_{\text{PCE}} = (\text{F-R})$	$\text{Jsc (mA/cm}^2\text{)}$	$\text{V}_{\text{oc}} (\text{V})$	FF (%)	PCE (%)	Ref.
MAPbI₃/HS	F		22.97	1.09	76.29	19.14	
	R	0.96	23.34	1.11	77.31	20.10	[14]
MAPbI₃/2,6-Py	F		22.85	1.07	77	18.82	
	R	0.59	23.14	1.09	77	19.41	[15]
CsFAMAPbIBr/KCl	F		22.98	1.11	74.94	19.2	
	R	0.22	23.01	1.13	74.02	19.4	[16]
CsFAMAPbIBr/MgO	F		23.71	1.12	78.91	21.08	
	R	0.17	23.86	1.12	78.76	20.91	[17]
MAPbI ₃ /dopedCLCS	F		22.7	1.06	80	19.3	
	R	n/a	n/a	n/a	n/a	n/a	[18]
FAPbI ₃ /PTQ10	F		22.84	1.12	80.24	20.58	
	R	0.63	23.15	1.12	82.57	21.21	[19]
MAPbI ₃ /PS	F		n/a	n/a	n/a	n/a	
	R	n/a	22.9	1.10	80.6	20.3	[20]
MAPbI ₃ /IDIC	F		n/a	n/a	n/a	n/a	
	R	n/a	22.96	1.11	76.53	19.5	[21]
CsFAMAPbIBr/CC	F		23.7	1.13	78	20.08	
	R	0.99	23.7	1.14	78	21.07	[22]
MAPbI ₃ /CdSe/ZnS	F		23.00	1.06	80.22	19.56	This
	R	0.33	23.18	1.06	81.44	19.89	work



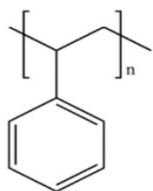
2,6-Dimethoxypyridine



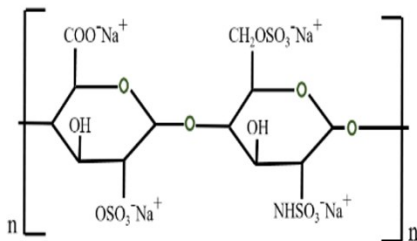
Choline chloride



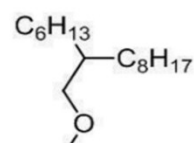
Potassium chloride (KCl)



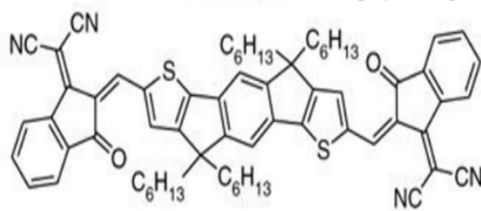
Polystyrene



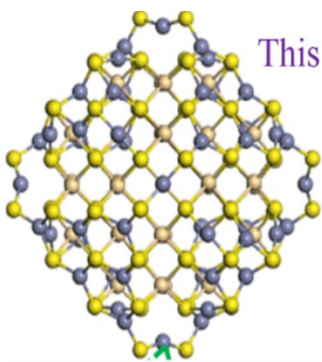
Biopolymer heparin sodium (HS)



PTQ10

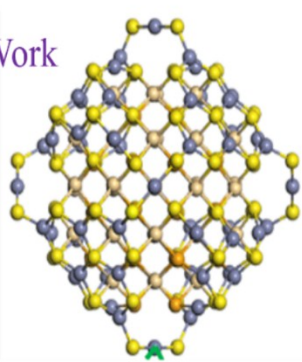


IDIC

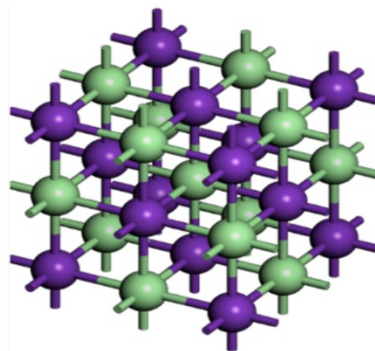


CdSe/ZnS

This Work



CdS/ZnS



Magnesium oxide (MgO)

Number of device	Scan direction	J_{sc} (mA/cm ²)	V_{oc} (V)	FF (%)	PCE (%)
1	F	23.00	1.06	80.22	19.56
	R	23.04	1.06	81.44	19.89
2	F	22.92	1.04	80.44	19.17
	R	23.11	1.04	80.10	19.25
3	F	22.00	1.04	83.09	19.01
	R	22.20	1.04	80.12	18.49
4	F	23.17	1.02	80.78	19.01
	R	23.20	1.01	81.00	18.97
5	F	23.50	0.98	78.02	17.96
	R	23.30	1	75.47	17.58
6	F	23.20	0.98	75.75	18.05
	R	23.20	1	79.42	17.57
7	F	23.50	1	75.75	17.50
	R	23.52	1	78.52	18.09
8	F	23.30	0.98	81.26	18.55
	R	23.40	1	80.34	18.79
9	F	23.01	0.99	75.68	17.24
	R	23.35	0.99	75.79	17.52
10	F	23.70	0.97	75.28	17.35
	R	23.77	0.97	77.37	17.83
11	F	23.50	0.97	78.57	17.91
	R	23.50	0.98	79.01	18.19
12	F	22.86	1.03	79	18.60
	R	22.91	1.05	78	18.76
13	F	22.49	1.04	80.05	18.72
	R	22.45	1.03	81.02	18.73
14	F	23.50	1.01	78	18.27
	R	23.30	1.02	79.02	18.77
15	F	22.95	1.01	80.12	18.57
	R	23.10	1.02	81.02	19.08
16	F	22.69	1.04	79	18.03
	R	22.85	1.04	80.12	18.37
17	F	22.75	1.02	77	17.86
	R	22.95	1.02	78	18.21
18	F	22.56	1.06	80.17	19.17
	R	22.62	1.05	80.43	19.34
19	F	22.28	1.04	79.80	18.49
	R	22.79	1.05	80.18	19.18
20	F	22.48	1.06	79.35	18.91
	R	22.76	1.06	79.64	19.21

Table S4: Photovoltaic parameters of PSCs incorporating a CdSe/ZnS Passivation layer.

Number of device	Scan direction	J_{sc} (mA/cm ²)	V_{oc} (V)	FF (%)	PCE (%)
1	F	20.90	1.00	74.94	15.66
	R	21.98	1.01	79.18	17.06
2	F	19.72	0.99	61.97	12.10
	R	20.41	1.00	76.77	15.67
3	F	21.22	1.00	76.67	16.27
	R	20.38	0.99	59.62	12.03
4	F	20.17	0.98	58.68	11.60
	R	21.00	0.98	76.72	15.79
5	F	19.42	0.97	74.42	14.02
	R	19.64	0.97	76.47	14.57
6	F	19.42	0.97	74.90	14.11
	R	19.65	0.97	76.70	14.62
7	F	20.71	0.91	64.94	12.24
	R	21.08	0.88	66.57	12.35
8	F	20.20	0.95	65.34	12.54
	R	20.94	0.92	66.90	12.89
9	F	19.72	0.92	65.59	11.90
	R	19.42	0.95	65.59	12.12
10	F	20.38	0.92	73.38	13.70
	R	20.61	0.89	77.19	14.16
11	F	18.30	0.93	69.48	11.91
	R	18.76	0.91	72.92	12.45
12	F	19.93	0.96	63.24	12.10
	R	20.48	0.93	65.94	12.56
13	F	20.27	0.93	71.77	13.53
	R	20.40	0.92	78.21	14.68
14	F	19.96	0.93	72.83	13.52
	R	20.07	0.90	77.61	14.02
15	F	20.26	0.94	69.78	13.29
	R	20.54	0.90	72.54	13.41
16	F	20.82	0.91	60.53	11.47
	R	21.20	0.94	76.47	15.24
17	F	19.89	0.99	64.44	12.69
	R	20.55	0.99	77.21	15.71
18	F	20.39	0.92	73.08	13.71
	R	20.52	0.88	76.08	13.74
19	F	19.85	0.99	68.03	12.69
	R	20.55	0.99	77.50	15.71
20	F	19.95	0.94	65.69	12.32
	R	20.50	0.93	77.71	14.79

Table S5: Photovoltaic parameters of PSCs incorporating a PCBM passivation layer.

Table S6: Photovoltaic parameters of PSCs with various active areas, incorporating a target passivation layer.

Active area	Scan direction	J_{sc} (mA/cm ²)	V_{oc} (V)	FF (%)	PCE (%)
0.1 cm ²	F	23.00	1.06	80.22	19.56
	R	23.18	1.06	81.44	20.01
0.5 cm ²	F	22.13	1.04	77.90	17.93
	R	22.31	1.04	80.37	18.65
1 cm ²	F	21.69	1.07	75.36	17.49
	R	22.03	1.06	79.82	18.64

Table S7: Hysteresis indices of PSCs with various dwelling times.

Dwelling time	Scan direction	J_{sc} (mA/cm ²)	V_{oc} (V)	PCE (%)	FF (%)	Hysteresis index(HI)
10 ms	R	22.87	1.03	18.77	79.68	0.4
	F	22.82	1.03	18.67	79.43	
100 ms	R	22.75	1.03	18.67	79.67	1.6
	F	22.64	1.03	18.48	79.24	
500 ms	R	22.09	1.01	17.66	79.15	3.48
	F	21.96	1.01	16.83	75.88	
1000 ms	R	21.79	1.01	17.59	79.92	7.99
	F	21.67	1.02	16.19	73.24	

Table S8: J-V parameters of PSCs devices passivated with CdSe/ZnS-TOPO and CdS/ZnS-OA QDs.

Passivation layer	Scan direction	J_{sc} (mA/cm ²)	V_{oc} (V)	FF	PCE (%)
CdSe/ZnS-TOPO	F	19.34	0.95	0.56	10.32
	R	20.5	0.97	0.71	14.16
CdS/ZnS-OA	F	17.49	0.93	0.62	10.11
	R	18.13	0.96	0.76	13.34

REFERENCES

- 1 K.M. Boopathi, R. Mohan, T.-Y. Huang, W. Budiawan, M.-Y. Lin, C.-H. Lee, K.-C. Ho, C.-W. Chu, *J. Mater. Chem. A*, 2016, **4**, 1591-1597.
- 2 X. Zhai, R. Zhang, J. Lin, Y. Gong, Y. Tian, W. Yang, X. Zhang, *Cryst. Growth Des.*, 2015, **15**, 1344-1350.
- 3 B.O. Dabbousi, J. Rodriguez-Viejo, F.V. Mikulec, J.R. Heine, H. Mattoussi, R. Ober, K.F. Jensen, M.G. Bawendi, *J. Phys. Chem. B*, 1997, **101**, 9463-9475.
- 4 C.-H. Hsia, A. Wuttig, H. Yang, *ACS Nano*, 2011, **5**, 9511-9522.
- 5 Z. Ning, X. Gong, R. Comin, G. Walters, F. Fan, O. Voznyy, E. Yassitepe, A. Buin, S. Hoogland, E.H. Sargent, *Nature*, 2015, **523**, 324.
- 6 H. Aqoma, M. Al Mubarak, W.T. Hadmojo, E.-H. Lee, T.-W. Kim, T.K. Ahn, S.-H. Oh, S.-Y. Jang, *Advanced Materials*, 2017, **29**, 1605756.
- 7 Z. Ning, H. Dong, Q. Zhang, O. Voznyy, E.H. Sargent, *ACS Nano*, 2014, **8**, 10321-10327.
- 8 S. Kanagasubbulakshmi, I. Gowtham, K. Kadirvelu, K. Archana, *MRS Communications*, 2019, **9**, 344-351.
- 9 N. Fernández-Delgado, M. Herrera, A.H. Tavabi, M. Luysberg, R.E. Dunin-Borkowski, P.J. Rodriguez-Cantó, R. Abargues, J.P. Martínez-Pastor, S.I. Molina, *Applied Surface Science*, 2018, **457**, 93-97.
- 10 M. Sytnyk, S. Yakunin, W. Schöfberger, R.T. Lechner, M. Burian, L. Ludescher, N.A. Killilea, A. YousefiAmin, D. Kriegner, J. Stangl, H. Groiss, W. Heiss, *ACS Nano*, 2017, **11**, 1246-1256.
- 11 A.A. Bessonov, M. Allen, Y. Liu, S. Malik, J. Bottomley, A. Rushton, I. Medina-Salazar, M. Voutilainen, S. Kallioinen, A. Colli, C. Bower, P. Andrew, T. Ryhänen, *ACS Nano*, 2017, **11**, 5547-5557.
- 12 Q. Dong, Y. Fang, Y. Shao, P. Mulligan, J. Qiu, L. Cao, J. Huang, *Science*, 2015, **347**, 967-970.
- 13 D. Shi, V. Adinolfi, R. Comin, M. Yuan, E. Alarousu, A. Buin, Y. Chen, S. Hoogland, A. Rothenberger, K. Katsiev, Y. Losovyj, X. Zhang, P.A. Dowben, O.F. Mohammed, E.H. Sargent, O.M. Bakr, *Science*, 2015, **347**, 519-522.
- 14 S. You, H. Wang, S. Bi, J. Zhou, L. Qin, X. Qiu, Z. Zhao, Y. Xu, Y. Zhang, X. Shi, H. Zhou, Z. Tang, *Adv. Mater.*, 2018, **30**, 1706924.
- 15 Y. Jiang, J. Li, S. Xiong, F. Jiang, T. Liu, F. Qin, L. Hu, Y. Zhou, *J. Mater. Chem. A*, 2017, **5**, 17632-17639.
- 16 X. Liu, Y. Zhang, L. Shi, Z. Liu, J. Huang, J.S. Yun, Y. Zeng, A. Pu, K. Sun, Z. Hameiri, J.A. Stride, J. Seidel, M.A. Green, X. Hao, *Adv. Energy Mater.*, 2018, **8**, 1800138.
- 17 J. Cao, B. Wu, R. Chen, Y. Wu, Y. Hui, B.-W. Mao, N. Zheng, *Advanced Materials*, 30 (2018) 1705596.
- 18 Y. Bai, Q. Dong, Y. Shao, Y. Deng, Q. Wang, L. Shen, D. Wang, W. Wei, J. Huang, *Nat. Commun.*, 2016, **7**, 12806.
- 19 L. Meng, C. Sun, R. Wang, W. Huang, Z. Zhao, P. Sun, T. Huang, J. Xue, J.-W. Lee, C. Zhu, Y. Huang, Y. Li, Y. Yang, *J. Am. Chem. Soc.*, 2018, **140**, 17255-17262.
- 20 Q. Wang, Q. Dong, T. Li, A. Gruverman, J. Huang, *Adv. Mater.*, 2016, **28**, 6734-6739.
- 21 Y. Lin, L. Shen, J. Dai, Y. Deng, Y. Wu, Y. Bai, X. Zheng, J. Wang, Y. Fang, H. Wei, W. Ma, X.C. Zeng, X. Zhan, J. Huang, *Adv. Mater.*, 2017, **29**, 1604545.
- 22 X. Zheng, B. Chen, J. Dai, Y. Fang, Y. Bai, Y. Lin, H. Wei, X. C. Zeng, J. Huang, *Nat. Energy*, 2017, **2**, 17102.